# Ultrasound Imaging: Correction of Geometric Distortions using Warping

Ari LEV-OR and Moshe PORAT
*Technion, Haifa 32000, Israel*
*re@vision.technion.ac.il mp@ee.technion.ac.il*

***Abstract* – Ultrasound images suffer from inherent geometric distortions due to variations in sound speed within the body. Other distortions include missing surfaces parallel to the direction of the ultrasonic rays, intense speckle noise, acoustic shadows and resolution inconsistency. These artifacts depend on the positioning of the transducer relative to the scanned organs, and considerably degrade the quality of the images obtained. We introduce a new algorithm that combines ultrasound images taken from distant viewpoints using spatial warping and compounding to obtain a quality-enhanced image. The algorithm is iterative: in each iteration the B-Mode images are divided into blocks and a matching procedure is performed between blocks of the reference images. Individual pixels are translated based on inter-block interpolation, subject to physical and medical constraints. The resultant warped images are used as an input signal to the next iteration. The algorithm was implemented and tested in-vitro, demonstrating superior results compared to presently available methods. The results are presented and discussed.**

***Index Terms* – Block Matching, Non-Linear Processing, Spatial Compounding, Ultrasound Imaging, 2D Warping.**

## I. INTRODUCTION

Ultrasound is a useful non-invasive tool for soft tissue imaging due to its low cost along with real time acquisition. The quality of the reconstructed images however is lower than in other medical imaging systems such as X-Ray, MRI or CT. It suffers from differences in spatial and axial resolution, noise (speckle and other), acoustic shadows, missing surfaces and geometric distortions.

One of the problems is the deformation caused by the variations in sound speed in the different body tissues. An ultrasound system assumes that the speed of sound is constant within the human body (1540 m/s) [5], and accordingly reconstructs the echoed pulses into a 2D image. It is known however that this speed varies [5] and causes the axial dimensions of organs to be out of scale (Figure 1). This variation in size however, despite its somewhat marginal effect on the resultant image, plays a major role when two or more ultrasound images are taken from different angles and compounded to create a higher quality image.

Previous works on image compounding, targeting speckle reduction and enhancing tissue boundaries, have either scanned the region of interest by alternately activating different parts of the poly-crystal transducer thus scanning in different angles [4], or used a mechanical arm to move [7] or track [3] the transducer with high accuracy. According to He's et al. approach [2], a thin wire phantom is used to calibrate the scanning system before performing the scan on a human subject.

In this work we propose a solution to the problem of geometric distortions based on image processing techniques. According to our proposed algorithm, two scans are obtained from two relatively distant viewpoints (Figure 2), resulting in significant geometric correction. Local information [6] is used for identifying similar parts in the two images, and an iterative process [1] warps the images to optimally match.

This work was supported in part by a grant from the GIF, the German-Israeli Foundation for Scientific Research and Development, and by the Ollendorff Minerva Center. Minerva is funded through the BMBF.

Fig. 1: Ultrasound images (simulation) of a circular cylinder. Left: The actual speed of sound inside the object is exactly as assumed. Different images are obtained if the speed inside the object is lower than assumed (center) or higher than assumed (right). The transducer is positioned at the top in all three images.

surfaces are also rectified by compounding two images, and will be discussed as byproducts of the proposed algorithm.

This paper is organized as follows. Definitions and notations are presented in Section II. The new algorithm is described in Section III, and major considerations are introduced in Section IV. Simulation results are given in Section V and the paper is concluded with a summary in Section VI.

## II. II. DEFINITIONS AND NOTATIONS

The following notations are used throughout this paper.

**2.1. Scan Line** – an A-Mode ultrasound image. Along this each pixel represents the intensity of the echoed (returned) pulse.

**2.2. Scan Line Collection Image (SLC Image)** – a raster display of the scan lines: the horizontal axis corresponds to the ultrasonic pulse firing-angle (i.e., angle of scan-line) and the vertical axis represents depth.

**2.3. Fan Image** - The B-Mode ultrasound image. This is a straightforward reconstruction of the image given the SLC image and the angle associated with each scan-line. The term 'Fan' indicates that the scan lines are in a fan-like arrangement.

**2.4. Difference between blocks**: The obtained images are gray-scale. The intensity of the pixel $(x, y)$ in block $k$ is represented by $I_k(x, y)$, where $0 \le x \le W-1$, and $0 \le y \le H-1$. $x, y, W, H \in \mathbf{Z}$ (integers). $W$ and $H$ denote the width and height of the block, respectively. The difference between two blocks is defined by

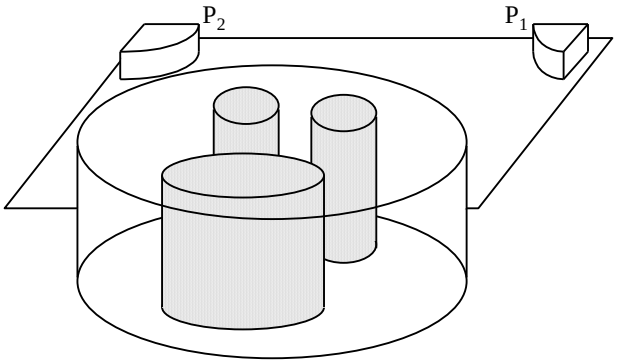


Fig. 2: The dual-transducer structure. The images obtained from two angles ($P_1$ and $P_2$) are integrated into a compounded higher quality image.

$$Diff_{jk} = \sum_{y=0}^{H-1}\sum_{x=0}^{W-1}\left|\frac{I_j(x,y)}{E_j} - \frac{I_k(x,y)}{E_k}\right| \quad (1)$$

where $E_j$ is related to the total energy (sum of pixel values) of block $j$:

$$E_j = \sum_{y=0}^{H-1}\sum_{x=0}^{W-1} I_j(x,y). \quad (2)$$

The difference *Diff* is in the range of [0, 2] due to normalization according to the size and energy of the blocks. *Diff=0* means that the blocks are identical, up to a multiplication factor, as in the case of acoustic shadows. Maximum difference *(Diff=2)* is obtained when each white pixel in the first image corresponds to a black pixel in the other, and vice versa. To avoid singularity, when a block is all black the result is set to *Diff=1*.

Equation (1) is also used for calculating the difference between the two images.

## III. THE ALGORITHM

Given the above definitions, we can now introduce the algorithm for spatial warping and compounding:

**3.1.** Acquire two SLC images of the same cross-section from two different viewpoints.

**3.2.** Construct two Fan images based on the two SLC images.

**3.3.** Rotate and translate the two Fan images according to the angle and displacement between the viewpoints.

**3.4.** Stop if the difference between two consecutive images is below a resolution threshold.

**3.5.** Divide both images into blocks. Calculate the spatial translation required for each block in each Fan image. Accordingly, derive the appropriate translation of all the pixels in each SLC image (Section 4).

**3.6.** Translate the pixels in both SLC images.

**3.7.** Go to step **3.2**.

These steps are summarized in Figure 3.

The algorithm is iterative. The two images are warped in each iteration to reduce the difference between them. The algorithm may be terminated in one of two ways: 1. After a predefined number of steps. 2. When the difference between the images is below a threshold value. The first approach is straightforward, and adequate.

## IV. IMAGE WARPING

The proposed algorithm is block based. Each image is divided into blocks, and a block-matching procedure is applied. The translation is calculated by averaging the translation of the block containing the pixel and the translation of the neighboring blocks. This process is carried out as follows.

**4.1**. Apply low-pass-filtering to both Fan images to reduce the sensitivity of the matching process to noise and contour deformation.

**4.2**. Divide the first fan image into blocks.

**4.3**. For each block perform block-matching between the two images. Two translation vectors are attained: A regular 2D minimum-difference translation, denoted $\vec{V}_{2D}$, and a vector of minimum-difference when translation is allowed only along the scan-line that goes through the block's center, denoted $\vec{V}_{SL}$. Consistency in the direction of these two vectors ensures that the deformation is only axial and is due to variations in sound speed.

**4.4**. Calculate a quality factor of the match $Q$ ($0 \le Q \le 1$): If $\vec{V}_{2D}$ and $\vec{V}_{SL}$ point in similar directions, the match is considered good and $Q$ is close to 1. Q is lower (close to 0) if the directions differ significantly. Denote the angle between the two vectors as $\theta$ (Figure 4), the quality factor is defined according to the projection of one vector onto another:

$$Q = \begin{cases} 0 & \cos(\theta) \le 0 \\ \cos(\theta) & \cos(\theta) > 0 \end{cases}. \quad (3)$$

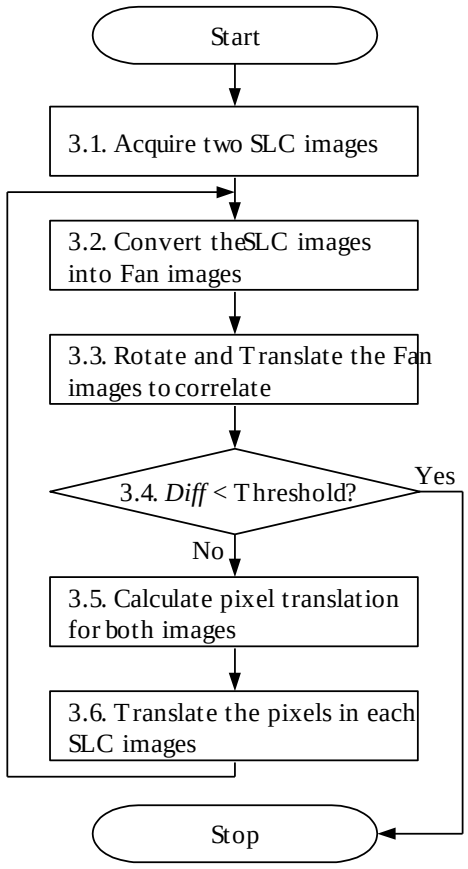


Fig. 3: Flowchart of the algorithm.

The quality factor serves as a weight of the block's translation when averaging translation of several blocks.

**4.5**. Calculate the final translation of the block. This translation must be *along* a scan-line assuming that the distortions due to speed variations are only axial. We define the final translation vector $\vec{V}_{final}$ to have the same direction

as $\vec{V}_{SL}$, and magnitude of $V_{final} = \min(V_{SL}, V_{2D} \cdot Q)$. By selecting the minimum translation over-warping of the image is avoided.

**4.6**. Once $\vec{V}_{final}$ is calculated for all the blocks, each pixel is translated according to the weighted average translation of its neighboring blocks. Two weights are applied when averaging: The quality factor *Q*, and the distance $D_n$ between the pixel and the block center.

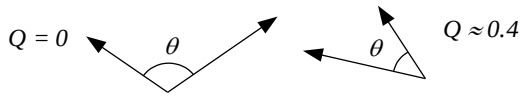


Fig. 4: Two examples of the quality factor Q. Left: θ>90° , cos(θ)<0 and Q=0. Right: θ<90° , cos(θ)>0 and Q>0.

Thus we get:

$$\vec{V}_{Pixel} = \frac{\sum_{n=0}^{8} \vec{V}_{n\,final} \cdot G(D_n) \cdot Q_n}{\sum_{n=0}^{8} G(D_n)} \quad , \tag{4}$$

where the weight function *G* is monotonically decreasing with the distance $D_n$:

$$G(D_n) = \begin{cases} 1 - \dfrac{D_n}{D_{Max}} & 0 \le D_n \le D_{Max} \\ 0 & D_n > D_{Max} \end{cases} \quad , \tag{5}$$

and

$$D_{Max} = 1.5\sqrt{W^2 + H^2} \quad . \tag{6}$$

$D_n$ and $D_{max}$ are measured in units of the sampling interval between pixels.

To avoid dependency on a specific block division we use overlapping block-sets that are displaced relative to the original division, i.e., the origin of the first (top-left) block is *(dx, dy)* instead of (0,0). The pixel translation process is performed on each block-set, thus eliminating a blockiness effect in the warped image.

## V. RESULTS

The algorithm was tested on the ultrasound images of Figure 2. The images are 256x256 pixels, each pixel is represented by 8 bits, i.e., 256 grey levels.

The first few iterations cause the difference between the images to decrease significantly (Figure 5). However, the iterative process may introduce an error since pixel translation is not necessarily according to an integer number and a single pixel may spread its energy in two neighboring pixels. Moreover, there is a mutual-pixel drift due to the feedback nature of the algorithm. The result is that after reaching a minimum, the difference between consecutive images may increase.

The algorithm was tested with regard to two parameters. The first parameter was the size of each block, ranging from $16^2$ to $56^2$ pixels, in steps of 8 pixels. The second parameter was the number of block-sets, selected in the range of 1 to $5^2$ (i.e., 5 subdivisions on each axis). According to our results, the algorithm is robust to the above changes if more than $2^2$ block-sets are used. It should be noted however that the image-difference is not related directly to image-quality as perceived by humans. For example, when using $16^2$-pixel blocks, the image-difference decreases rapidly to a low value, despite an intense blockiness effect and loss of contour roundness. Larger blocks ($32^2$ pixels and above) have shown slower decrease but the roundness of the contours was sustained.

## VI. SUMMARY

An image-processing technique has been applied successfully to ultrasound images, significantly reducing their inherent geometric distortions. The proposed algorithm is primarily designed to compensate for geometric distortions, however, a highly beneficial byproduct of the process is reduction of speckle noise and missing edges, since the combined image is an average of two images taken from distant viewpoints, in which the distortions diverse. It is also shown that the manipulation of the images is better done when using *both* SLC (scan line collection) and Fan (B-Mode) images.

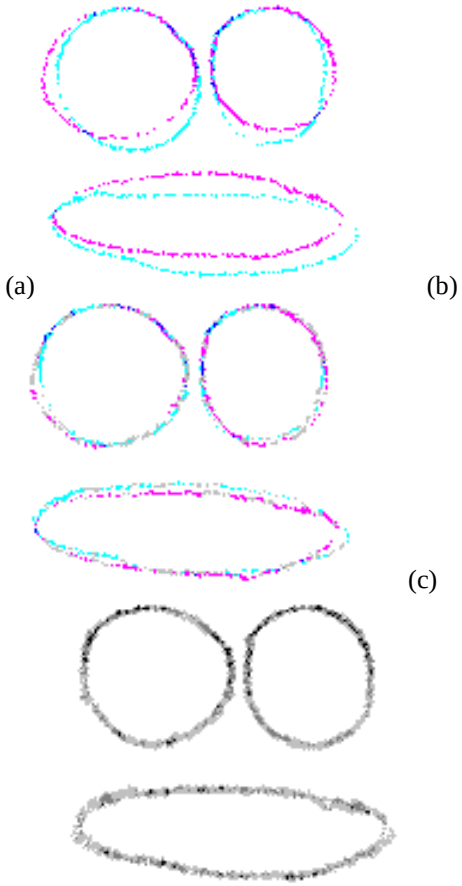


Fig.5: The compounded images according to the set-up of Figure 2. (a) The original two images. (b) After one iteration. (c) Minimum difference obtained after 8 iterations.

Our conclusion is that a dual-transducer system can significantly improve ultrasound imaging compared to the traditional approach. The new method may be also useful in correcting distortions caused by differences between lateral and radial resolutions, and may allow a wider ultrasonic beam thus achieving better defocusing property.

ACKNOWLEDGMENT

We thank Dr. Moshe Bronshtein of the *Al-Kol* ultrasound clinic in Haifa, Israel, for his contribution to this work. We are also grateful to Prof. I. Meizner and the staff of the Women-Ultrasound department of the *Belinson* Hospital (Rabin Medical Center), Petah-Tikva, Israel, for their assistance, and to Prof. Dan Adam of the Biomedical Engineering department at the Technion for his help. Lastly, we would like to thank Mr. Moti Shenhar, for the construction of the ultrasound phantom.

REFERENCES

[1] Y. Eldar, M. Lindenbaum, M. Porat and Y.Y. Zeevi, "The Farthest Point Strategy for Progressive Image Sampling", *IEEE Trans. On Image Processing*, Vol. 6, No. 9, pp. 1305-1315, 1997.

[2] P. He, K. Xue, P. Murka, "3-D imaging of residual limbs using ultrasound", *Journal of Rehabilitation Research and Development*, Vol. 34 No. 3, pp. 269-278, July 1997.

[3] A. Hernandez, O. Basset, P. Chirossel and G. Gimenez, "Spatial Compounding in Ultrasonic Imaging using an articulated scan arm", *Ultrasound in Medicine and Biology*, Vol. 22, No. 2, pp. 229-238, 1996.

[4] Soren K. Jespersen, Jens E. Wilhjelm and Henrik Sillesen, "Multi-Angle Compound Imaging", *Ultrasonic Imaging*, Vol. 20, pp. 81-102, 1998.

[5] "Biological Effects of Ultrasound: Mechanisms and Clinical Implications", *NCRP (National Council on Radiation Protection and Measurements) Report No. 74*, NCRP Publications, Bethesda, Maryland, Dec 30 1983.

[6] M. Porat and Y.Y. Zeevi, "Localized Texture Processing in Vision: Analysis and Synthesis in the Gaborian Space", *IEEE Trans. on Biomedical Engineering*, vol. BME-36, No. 1, pp. 115-129, 1989.

[7] Gregg E. Trahey, Stephen W. Smith, and Olaf T. Von Ramm, "Speckle Pattern Correlation with Lateral Aperture Translation: Experimental Results and Implications for Spatial Compounding", *IEEE Transactions on Ultrasonics and Frequency Control*, Vol. 33 No.3, pp. 257-264, May 1986.